Local infiltration of planar photonic crystals with UV-curable polymers

Pascale El-Kallassi,[1,*] Sandor Balog,[2] Romuald Houdré,[2] Laurent Balet,[2,3] Lianhe Li,[2] Marco Francardi,[4] Annamaria Gerardino,[4] Andrea Fiore,[3] Rolando Ferrini,[1] and Libero Zuppiroli[1]

[1]*Laboratoire d'Optoélectronique des Matériaux Moléculaires, Ecole Polytechnique Fédérale de Lausanne (EPFL), CH-1015 Lausanne, Switzerland*
[2]*Institut de Photonique et d'Electronique Quantique, Ecole Polytechnique Fédérale de Lausanne (EPFL), CH-1015 Lausanne, Switzerland*
[3]*COBRA Research Institute, Eindhoven University of Technology, NL-5600 MB Eindhoven, The Netherlands*
[4]*Institute for Photonics and Nanotechnologies, National Research Council (CNR), I-00156 Roma, Italy*
[*]*Corresponding author: pascale.el-kallassi@epfl.ch*

Received June 9, 2008; revised July 23, 2008; accepted July 23, 2008;
posted July 28, 2008 (Doc. ID 97133); published September 2, 2008

We present the local polymer infiltration of planar photonic crystal cavities via a maskless laser-writing technique. After the infiltration of the air holes with a UV-curable monomer a focused laser is used to locally polymerize the monomer in selected holes at the cavity boundaries. We show that cavity modes with different symmetries can be differently tuned depending on the size and the position of the infiltrated region around the cavity. © 2008 Optical Society of America

OCIS codes: 230.5298, 350.4238, 130.3120, 350.3450, 160.5470.

1. INTRODUCTION

In the past decade photonic crystals (PhCs) have been intensively studied as a promising platform for the fabrication of miniaturized optical devices whose potential has been demonstrated both theoretically and experimentally in several applied and fundamental fields such as, e.g., integrated optics and quantum optics [1,2]. Nowadays, PhC devices are routinely fabricated by locally modifying the structure of the air hole lattice [3]. Their optical properties can be optimized during the design procedure by modifying the size and/or the position of the air holes either inside or at the boundaries of the device [3]. Moreover, research efforts have been focused on the possibility of increasing the device functionality by either trimming or tuning the PhC optical properties after fabrication [4–14]. On one hand, the infiltration of the air holes with an organic material (e.g., liquid crystals or polymers) [4–8] has been demonstrated for both trimming and tuning. On the other hand, several theoretical studies have suggested that the selective infiltration of a few holes can provide an alternative approach for ultracompact photonic integrated components such as single mode waveguides, broadband low-reflection bends, crossings and splitters [9], or ultrahigh-Q cavities [10]. The potential of PhC infiltration with organic materials is thus amplified provided that a selective filling procedure is available. However, only a few examples of locally modified PhCs have been published so far [11–14]. For instance, Intonti *et al.* [11] have demonstrated microinfiltration of liquids in a macroporous silicon PhC via hollow submicrometer size pipettes and have suggested the possibility of nanoinfiltration with smaller microtips and UV imaging. Smith *et al.* [12] have used a similar technique to create a PhC double heterostructure based on the theoretical calculations by Tomljenovic-Hanic *et al.* [10]. Erickson *et al.* [13] have used nanofluidic targeting to infiltrate a single row of holes within a planar PhC using fluids with different refractive indices. More recently, Faraon *et al.* [14] have succeeded to locally tune GaAs-based PhC cavities by local photodarkening of a thin chalcogenide glass layer deposited on top of the device.

In this paper, we present an all-optical method to locally infiltrate air holes in a GaAs membrane PhC. This method exploits the local polymerization of an acrylate monomer by a UV laser and has been successfully used in the past to fabricate waveguiding devices in polymers [15]. In Section 2, we illustrate the optical properties of two-dimensional PhC cavities fabricated on a GaAs membrane. In Section 3, we describe the filling procedure, which consists of three steps: (i) infiltration of a PhC slab with a liquid monomer at room temperature and ambient atmosphere, (ii) local photopolymerization by focused UV-laser irradiation, and (iii) removal of the residual monomer from the unpolymerized PhC regions by organic solvents. Our technique presents several advantages: it does not require fine positioning of a micropipette or a nanochannel on the PhCs; it does not need the deposition of thick dielectric layers on the device surface that can eventually affect the optical properties of the planar PhC structure; the UV laser spot can be adjusted and moved to address any desired region; the refractive index of the infiltrated material can be chosen by selecting a molecule or a mixture of several molecules out of the large family of acrylates. In Section 4, we use this technique to trim the spectral response of the two-dimensional PhC cavities described in Section 2 by locally infiltrating their boundaries. We show how cavity modes with different symmetries can be differently tuned by choosing the size and the

position of the infiltrated region around the cavity. Scanning electron microscopy (SEM) and optical measurements are used to validate the filling procedure and to characterize locally infiltrated PhC cavities.

2. GaAs PHOTONIC CRYSTAL MEMBRANES

Planar PhCs consisting of a triangular lattice of air holes were fabricated by electron-beam lithography, CHF_3 plasma etching and $SiCl_4/O_2/Ar$ reactive ion etching through a 320 nm thick GaAs membrane grown by molecular beam epitaxy on top of a 1.5 μm thick $Al_{0.7}Ga_{0.3}As$ sacrificial layer. Details on the sample fabrication are given in [16]. A single layer of self-assembled InAs quantum dots (QDs: high areal density $\sim$ 300 dots/μm^2) [16] emitting around 1.3 μm was embedded in the membrane, thus enabling the optical characterization of the PhC structures by an internal light source technique [16]. The GaAs membrane is single mode for the TE polarization in the wavelength range of interest. The effective refractive index values $n_{eff}=3.151-3.038$ for the TE guided mode were calculated for $\lambda=1.2-1.4$ μm, respectively, by a transfer matrix method [17] and taking into account both the mode and the material dispersion.

PhC defect cavities were fabricated by removing three holes along the ΓK direction (i.e., $L3$ cavities) in the middle of a PhC slab placed at the center of a 12 μm diameter suspended membrane [see the inset of Fig. 1(a)]. The lattice constant and the hole diameter are $a=330$ nm and $d=202$ nm, respectively. This corresponds to an air filling factor $f=\pi d^2/2\sqrt{3}a^2=0.34$ (as measured on the SEM images) that, in the considered spectral region, yields a photonic bandgap only for the TE polarization [16].

To optically characterize the $L3$ cavities an internal light source technique with frontal collection was used [17,18]. A He–Ne pump laser emitting at 633 nm is focused in the center of the cavities (spot diameter $=2.5$ μm), so that the excited QD photoluminescence can couple to the cavity modes [18]. The scattered photoluminescence is collected through the same objective that focuses the pump beam and is used as a weak optical probe of the cavity modes [18]. The signal is then coupled to a multimode fiber whose conjugated image on the PhC surface has a diameter of 2.5 μm. This spot is focused in the center of the cavity as for the pump spot and the collected light is spectrally analyzed by means of a flat-field imaging spectrometer with a spectral resolution of 0.1 nm. The photoluminescence spectrum collected from an $L3$ cavity is shown in Fig. 1(a). Three peaks corresponding to the optical resonances excited inside the cavity appear at $\lambda_1=1130.7$ nm, $\lambda_2=1248$ nm, and $\lambda_3=1339.9$ nm. The resonance wavelengths of the TE cavity modes were calculated with a two-dimensional plane wave expansion (PWE) method assuming n_{eff} as the matrix refractive index [17]. Six cavity modes were found in the investigated spectral region. The resonance wavelengths calculated for $f=0.34$ (dashed lines) and their H_z-field maps are shown in Figs. 1(a) and 1(b), respectively. While peaks 1 and 3 correspond to a single cavity mode, peak 2 is the sum of four different resonances (2–1, 2–2, 2–3, and 2–4, in the increasing wavelength order), whose wavelengths are too close to be spectrally resolved. As is shown by the H_z-field maps, cavity modes 2–1, 2–2, and 2–4 are confined in the ΓK direction while modes 1 and 2–3 are confined in the ΓM direction. Cavity mode 3 is isotropically confined in both directions. Finally, we observe that cavity mode 1 is very close to the air band and its field partially leaks in the air holes. The peak indexing was confirmed by collecting the photoluminescence spectra for different orientations of a rotating polarizer placed in front of the detection system. The resonance wavelengths were fitted taking f as the fitting parameter. The value $f=0.34\pm0.01$ was obtained in agreement with the result of the SEM measurements.

The full widths at half-maximum (FWHMs) of the single resonance peaks 1 and 3 yield the cavity quality factors $Q_1=510\pm30$ and $Q_3=990\pm30$, respectively. These

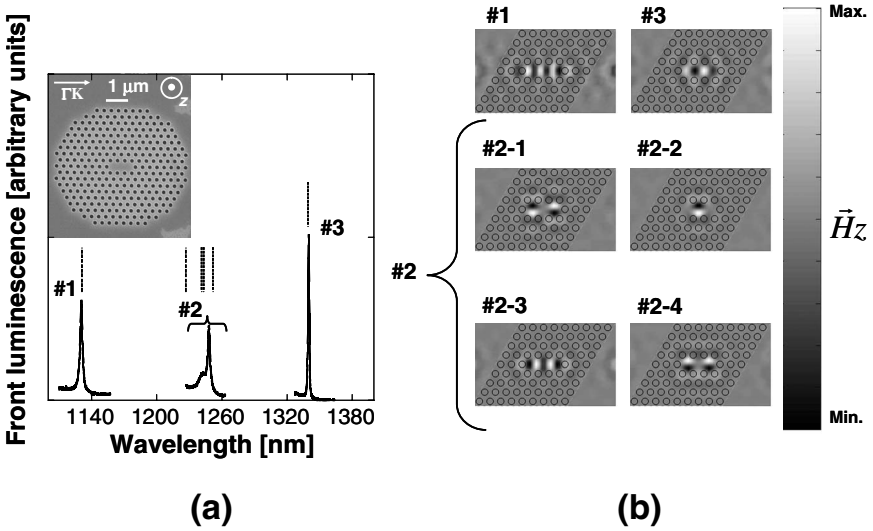

Fig. 1. (a) Front photoluminescence spectrum collected from an $L3$ cavity (see the SEM image in the inset: lattice constant $a=330$ nm and hole diameter $d=202$ nm). The resonance wavelengths of the TE cavity modes calculated for an air filling factor $f=0.34$ are shown (dashed lines). The ΓK lattice and the TE polarization (z) directions are indicated. (b) Calculated H_z-field maps of the TE cavity modes.

values agree with those found for similar unmodified $L3$ cavities on membranes [19] and are limited both by fabrication imperfections and by light reabsorption by the embedded QDs.

3. LOCAL INFILTRATION TECHNIQUE

The PhC structures were infiltrated with a liquid mixture of a dimethacrylate monomer (1,4-butanediol dimethacrylate) and 2% in weight of a photosensitive initiator [(1-hydroxycyclohexyl)phenyl-ketone] [see the chemical structures of the monomer and the photosensitive initiator in Fig. 2(b)]. The photosensitive initiator has three broad absorption peaks in the wavelength region 220–375 nm, and, when irradiated with UV light, it activates the free radical polymerization of the monomer. We remark that using a liquid monomer instead of a monomer in solution reduces the postpolymerization shrinkage typical of these materials (i.e., 10%–20% and 90% for a liquid monomer and a monomer in solution, respectively) [5].

The infiltration procedure is described in Fig. 2(a). The sample was immersed in the liquid mixture at room temperature and ambient atmosphere in order to completely cover the PhC patterns. The monomer wets completely the semiconductor–PhC surface (contact angle is $\sim 0°$), so that, as is discussed in [20], the hole infiltration is driven by the capillary forces. The velocity and the regime of the infiltration process depend on the liquid viscosity (7 cps $=0.007$ Pa·s. in our case) [20,21]. We remark that, following the same procedure as in [4], the hole filling was checked by optical measurements. After the monomer infiltration, the wavelength shift of the cavity resonance peaks was measured and fitted taking the value measured by ellipsometry for the monomer refractive index ($n=1.39\pm0.01$ at $\lambda=1.3$ μm). Assuming the hole refractive index n_{hole} as the fitting parameter we obtained $n_{\text{hole}}=1.38\pm0.02$ that corresponds to an infiltration efficiency of $95\%\pm5\%$ [4].

After the monomer infiltration, the sample was removed from the bath and fixed on a sample holder for the polymerization step. An Ar-ion laser emitting at 351 nm was focused on the PhC. The UV-activated polymerization was performed under a N_2 flow in order to prevent the radicals formed during the process from reacting with the O_2 molecules thus stopping the polymerization [22]. The irradiation power and time were adjusted so as to obtain a complete polymerization over the thickness of the infiltrated holes. After the selective polymerization, the residual monomer was removed from the unpolymerized PhC regions using organic solvents (acetone and isopropanol).

By adjusting the UV-laser spot diameter (e.g., from 5 to 1 μm), the size of the infiltrated PhC region can be controlled on a micrometer scale and reduced from a few tens of holes down to ten or less. The SEM top-view and cross-section images of the $L3$ cavity globally infiltrated over a 5.2 μm region are shown in Figs. 3(a) and 3(e), respectively. In this case, a residual polymer layer remains under the membrane. By dividing the cross section of this polymer underlayer over the cross section of the underlying cavity, a polymer shrinkage of the order of 20% can be roughly estimated that agrees with the typical 10%–20% shrinkage expected for this family of acrylates [5]. The possibility of selectively polymerizing a 1.2–1.8 μm area in close vicinity to a $L3$ cavity is demonstrated in Figs. 3(b) and 3(c). A residual polymer overlayer with a thickness of the order of tens nm may remain above the membrane as it is shown in the tilted top-view SEM image in Fig. 3(d). We remark that this overlayer as well as the underlayer shown in Fig. 3(e) do not extend beyond the locally polymerized area, thus not affecting the PhC optical properties.

4. OPTICAL CHARACTERIZATION AND DATA ANALYSIS

The infiltrated cavities were optically characterized in order to validate the filling procedure. The photolumines-

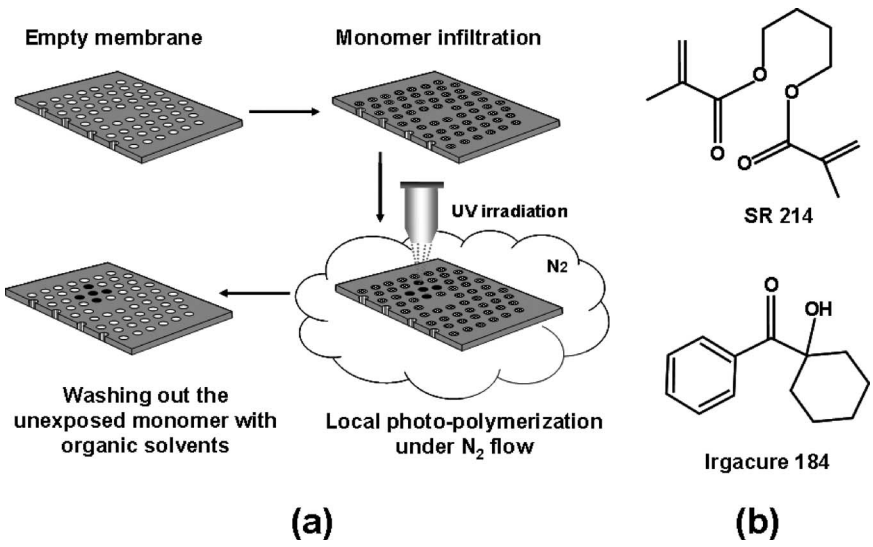

Fig. 2. (a) Local infiltration procedure. After infiltration with a liquid monomer a UV laser is focused on the photonic crystal inducing local polymerization of the monomer inside the selected holes. The monomer is then removed from the other holes by washing the sample in organic solvents. (b) Chemical structures of the dimethacrylate monomer SR214 (1,4-butanediol dimethacrylate) and of the photosensitive initiator Irgacure 184 [(1-hydroxycyclohexyl)phenyl-ketone].

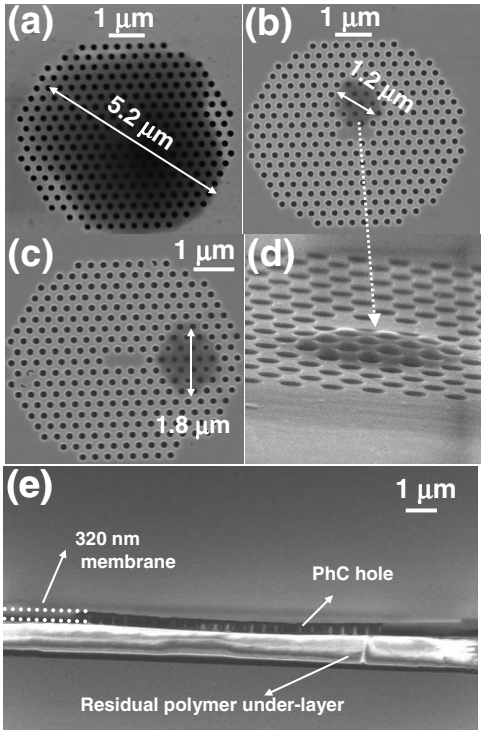

Fig. 3. SEM images of the infiltrated photonic crystal structure after local polymerization and monomer removal: (a)–(c) top-view images of the $L3$ cavity globally (filled area diameter=5.2 μm) and locally (filled area diameter=1.2 and 1.8 μm) infiltrated, respectively; (d) tilted top-view image of the locally infiltrated cavity shown in (b); (e) cross-section image of the globally infiltrated cavity shown in (a).

cence spectrum collected from the $L3$ cavity of Fig. 3(a) is shown in Fig. 4. When the cavity boundaries are globally infiltrated the photonic bandgap shrinks and the resonance peaks (solid curves) redshift with respect to the empty cavity (dashed curves) due to the reduced refractive index difference between the holes and the semiconductor. The resonance peaks are located at $\lambda_2=1292$ nm and $\lambda_3=1367.3$ nm for resonances 2 and 3, respectively, while peak 1 disappears because of the gap shrinkage (see Fig. 4). To compare the experimental resonance wavelengths with theoretical PWE calculations, the n_{eff} value was recalculated taking into account the residual polymer overlayer and underlayer [see Figs. 3(d) and 3(e)]. The polymer refractive index was measured by spectroscopic ellipsometry ($n=1.51\pm0.01$ at $\lambda=1.3$ μm) and the value $n_{eff}=3.1051\pm0.0004$ is obtained at $\lambda=1.3$ μm for a membrane completely embedded into the polymer. Assuming the latter n_{eff} value as the matrix refractive index, PWE calculations were performed with the refractive index n_{hole} inside the holes as the fitting parameter. The value $n_{\text{hole}}=1.40\pm0.02$ was obtained that yields an average filling efficiency [4] of 80% in agreement with the value estimated from the cross-section SEM image in Fig. 3(e).

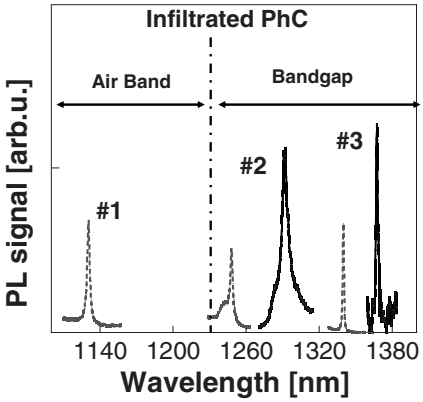

Fig. 4. Front photoluminescence (PL) spectrum collected from the globally infiltrated $L3$ cavity shown in Fig. 3(a) (solid curves). The resonance peaks for the corresponding empty cavity are shown as references (dashed curves) as well as the bandgap and the air band boundaries for the filled photonic crystal.

The resonance quality factors decrease with respect to the empty cavity (e.g., $Q_3'=769$ with $\Delta Q/Q=20\%$). This should be mainly due to the reduced refractive index difference between the holes and the semiconductor membrane, and thus to the reduced reflectivity of the PhC boundaries. In this particular case, the presence of the polymer overlayer and underlayer might also contribute to the decrease of the cavity quality factor.

The photoluminescence spectrum collected from the $L3$ cavity of Fig. 3(b) is shown in Fig. 5. When the cavity boundaries are locally infiltrated, the redshift of the resonance peaks is of the order of a few nanometers: i.e., $\Delta\lambda=1-10$ nm, depending on the considered resonance peak. These experimental values agree very well with the values calculated with the PWE model using the n_{eff} value calculated for the bare membrane (i.e., with no polymer overlayer and underlayer) and taking an $L3$ cavity with the same ten-hole infiltrated region as the one shown in Fig. 3(b). Moreover the theoretical calculations clearly show that, since the infiltrated region lies in the ΓM direction with respect to the $L3$ cavity axis, the redshift is larger for the modes confined in the ΓK direction than for those confined in the ΓM direction: i.e., $\Delta\lambda=6-10$ nm and $\Delta\lambda=1-3$ nm for the ΓK (2–1, 2–2, and 2–4) and the ΓM (1 and 2–3) confined modes, respectively [see also Fig. 1(b)]. Note that the apparent doublet structure of resonance 1 is not due to a mode splitting but to the shift of an air band mode into the gap (see the inset of Fig. 5) [23]. We remark that, in spite of the nanometer-scale tuning of the resonance wavelengths, for the modes that remain well-confined into the cavity (e.g., 3), since in this case the local infiltration leaves the boundary reflectivity almost unaffected, the resonance quality factor remains constant with respect to the empty cavity: e.g., $Q_3''=985$.

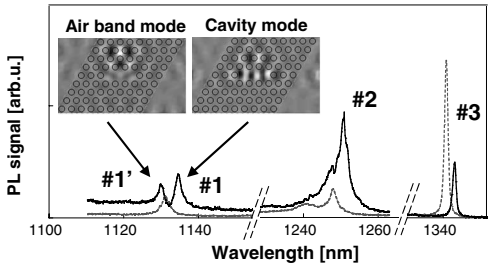

Fig. 5. Front photoluminescence (PL) spectrum collected from the $L3$ cavity with locally infiltrated boundaries in the ΓM direction shown in Fig. 3(b) (solid curves). The resonance peaks for the corresponding empty cavity are shown as references (dashed curves). The H_z-field maps calculated for cavity 1 and air band 1′ modes are shown.

The photoluminescence spectrum collected from the $L3$ cavity of Fig. 3(c) is shown in Fig. 6. In this case, due to the position of the locally infiltrated area and the reduced leakage of the cavity modes in the ΓK direction with respect to the ΓM direction [see Fig. 1(b)], the resonance redshift is lower than that measured for the cavity of Fig. 3(b), i.e., $\Delta\lambda = 0.1-3$ nm depending on the considered resonance peak. Again the experimental values agree very well with the values calculated with the PWE method used above taking an $L3$ cavity with the same 20-hole infiltrated region as the one shown in Fig. 3(c). In this case, since the infiltrated region lies in the ΓK direction with respect to the $L3$ cavity axis, the redshift is larger for the modes confined in the ΓM direction than for those confined in the ΓK direction: i.e., $\Delta\lambda = 1-3$ nm and $\Delta\lambda = 0.1-0.3$ nm for the ΓM (1 and 2–3) and the ΓK (2–1, 2–2, and 2–4) confined modes, respectively [see also Fig. 1(b)]. Therefore we have demonstrated the possibility to address differently cavity modes with different symmetries by adjusting the position and the size of the locally infiltrated area around the cavity. Finally, as in Fig. 5, the apparent doublet structure of resonance 1 is due to the shift of an air band mode into the gap (see the inset of Fig. 6).

5. CONCLUSIONS

In conclusion, we have demonstrated the local polymer infiltration of planar PhC devices. In particular, we have exploited the local photopolymerization of PhC cavities infiltrated with a liquid dimethacrylate monomer to selectively fill the cavity boundaries over PhC regions ranging from 5 down to 1 μm. An internal light source technique was used to measure the shift of the cavity resonances after the local infiltration. The experimental measurements were compared to theoretical PWE calculations showing that the wavelength shifts correspond well to the refractive index change in the infiltrated PhC region. By adjusting the size and the position of the infiltrated area around the cavity, we were able to tune differently cavity modes of different symmetry.

Our local infiltration method has several advantages: the shape of the infiltrated area can be easily and reproducibly controlled by moving the UV laser spot on the PhC surface and since the size of the polymerized area depends mainly on the size of the UV spot (that can be reduced to a few hundreds of nanometers), the infiltration of single air holes over a PhC device can be straightforwardly achieved. We highlight that, apart from acrylates, there is a large variety of optical polymers [24,25] that can be used to achieve local infiltration with our technique, provided that the chosen material meets the right (i) infiltration (e.g., good wetting, molecule size versus hole diameter) and (ii) physicochemical (e.g., limited shrinkage after polymerization) properties.

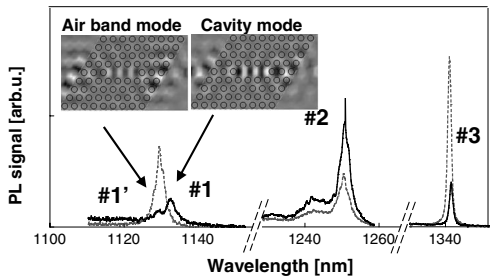

Fig. 6. Front photoluminescence (PL) spectrum collected from the $L3$ cavity with locally infiltrated boundaries in the ΓK direction shown in Fig. 3(c) (solid curves). The resonance peaks for the corresponding empty cavity are shown as references (dashed curves). The H_z-field maps calculated for cavity 1 and air band 1′ modes are shown.

ACKNOWLEDGMENTS

The authors thank N. Le Thomas, M. Schär from the Ecole Polytechnique Fédérale de Lausanne (EPFL, Switzerland), and M. Hofmann from 3D Systems S.A. (Marly, Switzerland) for their help. This work was performed within the framework of the European Network of Excellence on Photonic Integrated Components and Circuits (ePIXnet) and the Swiss National Center of Competence in Research (NCCR) in Quantum Photonics.

REFERENCES

1. J. M. Lourtioz, H. Benisty, V. Berger, J. M. Gérard, D. Maystre, and A. Tchelnokov, *Photonic Crystals* (Springer, 2005).
2. K. Busch, S. Lölkes, R. B. Wehrspohn, and H. Föll, *Photonic Crystals* (Wiley-VCH, 2004).
3. B-S. Song, S. Noda, T. Asano, and Y. Akahane, "Ultra-high-Q photonic double-heterostructure nanocavity," Nat. Mater. **4**, 207–210 (2005).
4. R. Ferrini, J. Martz, L. Zuppiroli, B. Wild, V. Zabelin, L. A. Dunbar, R. Houdré, M. Mulot, and S. Anand, "Planar photonic crystals infiltrated with liquid crystals: tuning and optical characterization of molecule orientation," Opt. Lett. **31**, 1238–1240 (2006).
5. R. van der Heijden, C.-F. Carlström, J. Snijders, R. W. van der Heijden, F. Karouta, R. Nötzel, H. Salemink, C. Kjellander, C. Bastiaansen, D. Broer, and E. van der Drift, "InP-based two-dimensional photonic crystals filled with polymers," Appl. Phys. Lett. **88**, 161112 (2006).
6. S. Tay, J. Thomas, B. Momeni, M. Askari, A. Adibi, P. J. Hotchkiss, S. C. Jones, S. R. Marder, R. A. Norwood, and N. Peyghambarian, "Planar photonic crystals infiltrated with nanoparticle/polymer composites," Appl. Phys. Lett. **91**, 221109 (2007).
7. M. Haurylau, S. P. Anderson, K. L. Marshall, and P. M. Fauchet, "Electrically tunable silicon 2-D photonic bandgap structures," IEEE J. Quantum Electron. **12**, 1527–1533 (2006).
8. P. Barthelemy, M. Ghulinyan, Z. Gaburro, C. Toninelli, L. Pavesi, and D. Wiersma, "Optical switching by capillary condendation," Nat. Photonics **1**, 172–175 (2007).
9. S. Mingaleev, M. Schillinger, D. Hermann, and K. Busch, "Tunable photonic crystal circuits: concepts and designs based on single-pore infiltration," Opt. Lett. **29**, 2858–2860 (2004).
10. S. Tomljenovic-Hanic, C. Martijn de Sterke, and M. J. Steel, "Design of high-Q cavities in photonic crystal slab heterostructures by air-holes infiltration," Opt. Express **14**, 12451–12456 (2006).
11. F. Intonti, S. Vignolini, V. Türck, M. Colocci, P. Bettotti, L. Pavesi, S. L. Schweizer, R. Wehrspohn, and D. Wiersma, "Rewritable photonic circuits," Appl. Phys. Lett. **89**, 211117 (2006).
12. C. L. C. Smith, D. K. C. Wu, M. W. Lee, C. Monat, S. Tomljenovic-Hanic, C. Grillet, J. Eggleton, D. Freeman, Y. Ruan, S. Madden, B. Luther-Davies, H. Giessen, and Y-H. Lee, "Microfluidic photonic crystal double heterostructure," Appl. Phys. Lett. **91**, 121103 (2007).

13. D. Erickson, T. Rockwood, T. Emery, A. Scherer, and D. Psaltis, "Nanofluidic tuning of photonic crystal circuits," Opt. Lett. **31**, 59–61 (2006).
14. A. Faraon, D. Englund, D. Bulla, B. Luther-Davies, B. J. Eggleton, N. Stoltz, P. Petroff, and J. Vučković, "Local tuning of photonic crystal cavities using chalcogenide glasses," Appl. Phys. Lett. **92**, 043123 (2008).
15. L. Eldada, C. Xu, K. M. T. Stengel, L. W. Schacklette, and J. T. Yardley, "Laser-fabricated low-loss single mode raised-rib waveguiding devices in polymers," J. Lightwave Technol. **14**, 1704–1713 (1996).
16. A. Gerardino, M. Francardi, L. Balet, C. Monat, C. Zinoni, B. Alloing, L. H. Li, N. Le Thomas, R. Houdré, and A. Fiore, "Fabrication and characterization of point defect photonic crystal nanocavities for telecom-wavelength," Microelectron. Eng. **84**, 1480–1483 (2007).
17. R. Ferrini, D. Leuenberger, M. Mulot, M. Qiu, J. Moosburger, M. Kamp, A. Forchel, S. Anand, and R. Houdré, "Optical study of two-dimensional InP-based photonic crystals by internal light source technique," IEEE J. Quantum Electron. **38**, 786–799 (2002).
18. C. J. Smith, T. F. Krauss, H. Benisty, M. Rattier, C. Weisbuch, U. Oesterle, and R. Houdré, "Directionally dependent confinement in photonic-crystal microcavities," J. Opt. Soc. Am. B **17**, 2043–2051 (2000).
19. M. Francardi, L. Balet, A. Gerardino, C. Monat, C. Zinoni, L. H. Li, B. Alloing, N. Le Thomas, R. Houdré, and A. Fiore, "Quantum dot photonic crystal nanocavities at 1300 nm for telecom-wavelength single-photons sources," Phys. Status Solidi C **3**, 3693–3696 (2006).
20. K. Nielsen, D. Noordegraaf, T. Sørensen, A. Bjarklev, and T. P. Hansen, "Selective filling of photonic crystal fibers," J. Opt. A, Pure Appl. Opt. **7**, L13–L20 (2005).
21. O. Kriha, L. Zhao, E. Pippel, U. Gösele, R. B. Wehrspohn, J. H. Wendorff, M. Steinhart, and A. Greiner, "Organic tube/rod hybrid nanofibers with adjustable segment lengths by bidirectional template wetting," Adv. Funct. Mater. **17**, 1327–1332 (2007).
22. K. Studer, C. Decker, E. Beck, and R. Schwalm, "Overcoming oxygen inhibition in UV-curing of acrylate coatings by carbon dioxide inerting, Part I," Prog. Org. Coat. **48**, 92–100 (2003).
23. R. P. Stanley, R. Houdré, U. Oesterle, M. Ilegems, and C. Weisbuch, "Impurity modes in one-dimensional periodic systems: the transition from photonic band gaps to microcavities," Phys. Rev. A **48**, 2246–2250 (1993).
24. H. Ma, A. K.-Y. Jen, and L. R. Dalton, "Polymer-based optical waveguides: materials, processing and devices," Adv. Mater. (Weinheim, Ger.) **14**, 1339–1365 (2002).
25. M. Chanda and S. K. Roy, *Plastics Technology Handbook* (CRC, 2007).